

Controllable high Curie temperature through 5d transition metal atom doping in CrI_3

Xuebing Peng(彭雪兵), Mingsu Si(司明苏), and Daqiang Gao(高大强)
Citation: Chin. Phys. B, 2024, 33 (**1**): 017503. DOI: 10.1088/1674-1056/ad053b
Journal homepage: http://cpb.iphy.ac.cn; http://iopscience.iop.org/cpb

What follows is a list of articles you may be interested in

Low-temperature ferromagnetism in tensile-strained $LaCoO_{2.5}$ thin film

Yang-Yang Fan(范洋洋), Jing Wang(王晶), Feng-Xia Hu(胡凤霞), Bao-He Li(李宝河), Ai-Cong Geng(耿爱丛), Zhuo Yin(殷卓), Cheng Zhang(张丞), Hou-Bo Zhou(周厚博), Meng-Qin Wang(王梦琴), Zi-Bing Yu(尉紫冰), and Bao-Gen Shen(沈保根)
Chin. Phys. B, 2023, 32 (**8**): 087504. DOI: 10.1088/1674-1056/acafdc

Out-of-plane weak ferromagnetism at room temperaturein lattice-distortion non-collinear antiferromagnet of single-crystal Mn_3Sn

Bo-Xi Zhang(张博熙), Ping Song(宋平), Shan-Shan Deng(邓珊珊), Li Lou(娄理), and Sen Yao(姚森)
Chin. Phys. B, 2023, 32 (**8**): 087502. DOI: 10.1088/1674-1056/acca0b

Prediction of $LiCrTe_2$ monolayer as a half-metallic ferromagnet with a high Curie temperature

Li-Man Xiao(肖丽蔓), Huan-Cheng Yang(杨焕成), and Zhong-Yi Lu(卢仲毅)
Chin. Phys. B, 2023, 32 (**5**): 057505. DOI: 10.1088/1674-1056/acbe2e

A spin-based magnetic scanning microscope for *in-situ* strain tuning of soft matter

Zhe Ding(丁哲), Yumeng Sun(孙豫蒙), Mengqi Wang(王孟祺), Pei Yu(余佩), Ningchong Zheng(郑宁冲), Yipeng Zang(臧一鹏), Pengfei Wang(王鹏飞), Ya Wang(王亚), Yuefeng Nie(聂越峰), Fazhan Shi(石发展), and Jiangfeng Du(杜江峰)
Chin. Phys. B, 2023, 32 (**5**): 057504. DOI: 10.1088/1674-1056/acbaee

Dynamical signatures of the one-dimensional deconfined quantum critical point

Ning Xi(西宁) and Rong Yu(俞榕)
Chin. Phys. B, 2022, 31 (**5**): 057501. DOI: 10.1088/1674-1056/ac5987

Controllable high Curie temperature through 5d transition metal atom doping in CrI_3

Xuebing Peng(彭雪兵)[1], Mingsu Si(司明苏)[2], and Daqiang Gao(高大强)[1,†]

[1] *School of Physical Science and Technology, Lanzhou University, Lanzhou* 730000, *China*
[2] *School of Materials and Energy, Lanzhou University, Lanzhou* 730000, *China*

(Received 4 July 2023; revised manuscript received 26 September 2023; accepted manuscript online 20 October 2023)

Two-dimensional (2D) CrI_3 is a ferromagnetic semiconductor with potential for applications in spintronics. However, its low Curie temperature (T_c) hinders realistic applications of CrI_3. Based on first-principles calculations, 5d transition metal (TM) atom doping of CrI_3 (TM@CrI_3) is a universally effective way to increase T_c, which stems from the increased magnetic moment induced by doping with TM atoms. T_c of W@CrI_3 reaches 254 K, nearly six times higher than that of the host CrI_3. When the doping concentration of W atoms is increased to above 5.9%, W@CrI_3 shows room-temperature ferromagnetism. Intriguingly, the large magnetic anisotropy energy of W@CrI_3 can stabilize the long-range ferromagnetic order. Moreover, TM@CrI_3 has a strong ferromagnetic stability. All TM@CrI_3 change from a semiconductor to a half-metal, except doping with Au atom. These results provide information relevant to potential applications of CrI_3 monolayers in spintronics.

Keywords: ferromagnetism, magnetic anisotropy energy, Curie temperature, half-metal

PACS: 75.50.Pp, 71.15.Mb, 71.20.–b **DOI:** 10.1088/1674-1056/ad053b

1. Introduction

Although two-dimensional (2D) materials have been explored for more than a decade, magnetic order rarely survives in atomically thin films due to thermal fluctuations.[1,2] The realization of 2D magnets is a big challenge. An early strategy was to introduce local defect states with magnetic elements into non-magnetic materials.[3–6] The magnetism introduced by this method is short-range. A new method to achieve low-dimensional ferromagnets is to use intrinsic magnetic order. In 2017, monolayer CrI_3 and few-layer $Cr_2Ge_2Te_6$ were simultaneously reported.[7,8] Immediately afterwards, in 2018, Deng *et al.* successfully prepared monolayer Fe_3GeTe_2 with intrinsic ferromagnetism.[9] These works opened the door for the study of 2D magnetic materials and provided a novel material platform for the future development of low-dimensional spintronics.

CrI_3 as a layered magnetic material was first systematically studied by Dillon and Olson[10] and realized in the monolayer limit by Huang *et al.*[7] A spin-orientation-controlled band structure offers the opportunity for the study of second harmonics in solid state physics.[13,14] Due to its special crystal structure, CrI_3 has a topologically protected spin magnetic moment[15] as well as Kitaev interaction induced by shared edge I^-.[16] With a strong layer-dependent effect, the magnetic ground state can be changed from ferromagnetic (FM) to antiferromagnetic (AFM) as the monolayer becomes a bilayer.[17] The excellent magnetism of CrI_3 makes it potentially promising for applications in the field of spintronics. Most research is based on the intrinsic magnetism of CrI_3. However, the Curie temperature (T_c) of CrI_3 is only 45 K,[18] which severely limits its practical applications. Thus, increasing the T_c of CrI_3 is a focus of research.

The magnetism of monolayer CrI_3 has been modulated by strain,[19,20] carrier doping,[21] defect introduction,[22,23] applied electric field[24] and surface adsorption.[25–27] For example, Guo *et al.* adsorbed Li atoms on the surface to semimetallize CrI_3 and increase T_c.[28] Yang *et al.* used Sc atoms to dope CrI_3 and increased T_c from 47 K to 131 K.[29] The gain or loss of electrons causes an increase in the magnetic moment of Cr, which eventually increases T_c. In fact, the above methods are not particularly effective ways to increase T_c because Li and Sc atoms have almost no magnetic moment in a honeycomb lattice. Recently, Birgeneau's group successfully prepared Fe_5GeTe_2, which has a higher T_c (over 400 K) than Fe_3GeTe_2. The underlying physics originates from the increasing coordination number of the Fe ion.[30] Based on the above ideas, we chose 5d transition metal (TM) atoms to dope CrI_3, because 5d TM atoms with a larger spin–orbit coupling (SOC) may increase the magnetic anisotropy energy (MAE) to stabilize long-range FM order.

In this work, we investigate the crystal stability, MAE, T_c, FM stability and electronic properties of TM@CrI_3 based on first-principles calculations. Formation energy and phonon spectra calculations show that TM@CrI_3 is thermodynamically stable, and the absence of imaginary modes in phonon spectra indicates that TM@CrI_3 monolayers (TM = Hf, Ta, W, Re and Os) are also dynamically stable. Due to the in-

†Corresponding author. E-mail: gaodq@lzu.edu.cn

© 2024 Chinese Physical Society and IOP Publishing Ltd

crease in magnetic moment induced by the doping of TM atoms, TM@CrI_3 has a higher T_c through Monte–Carlo (MC) simulation. Among these, T_c of W@CrI_3 reaches 254 K. By further increasing the doping concentration of W atoms, a T_c above room temperature can be achieved. Intriguingly, a large MAE for W@CrI_3 can stabilize long-range FM order. Moreover, FM stability of TM@CrI_3 is enhanced. Most TM@CrI_3 change from a semiconductor to a half-metal. These results provide knowledge relevant to potential applications of CrI_3 monolayers in spintronics.

2. Computational details

We use the framework of density functional theory as implemented in the Vienna *ab initio* simulation package to perform first-principles calculations.[31,32] The Monkhorst–Pack scheme of $5\times5\times1$ k-point sampling in the entire Brillouin zone (BZ) was used to perform momentum space integration for a $2\times2\times1$ TM@CrI_3 supercell.[33] MAE was calculated with a $12\times12\times1$ k-point mesh. The plane-wave cutoff energy was set to 500 eV. The generalized gradient approximation with the Perdew–Burke–Ernzerhof realization was used for the exchange correlation functional.[34] The Hellmann–Feynman forces acting on each atom were entirely relaxed during structural optimization until they were less than 10^{-3} eV·Å^{-1}; the electronic convergence requirement was set to 10^{-7} eV. Since the system is a 2D nanosheet, a vacuum region of 20 Å along the direction perpendicular to the surface of the nanosheet was introduced to avoid interference between the periodic images. A $30\times30\times1$ supercell was used to simulate T_c based on the MC method.[35]

3. Results and discussion

Monolayer CrI_3 possesses the space group of p-31m (No. 162). Cr^{3+} ions are sandwiched by octahedra formed by shared-edge I^- ions and form a hexagonal honeycomb structure, as shown in Fig. 1(a). The optimized lattice constant is $a=b=7.00$ Å. The Cr^{3+}–I^- and Cr^{3+}–Cr^{3+} bond distances are 2.7 Å and 4.0 Å, respectively. The magnetic moment of each Cr^{3+} ion is 3.06 μ_B. The band structure of CrI_3 is displayed in Fig. 1(b). The valence band maximum and the conduction band minimum appear for the spin-up channel, giving a band gap of 1.21 eV. All these results are in good agreement with previously reported results.[29,36] Here, we dope CrI_3 with one 5d TM atom, introducing it into the interstitial hollow position of a $2\times2\times1$ supercell, as shown in Fig. 1(c).

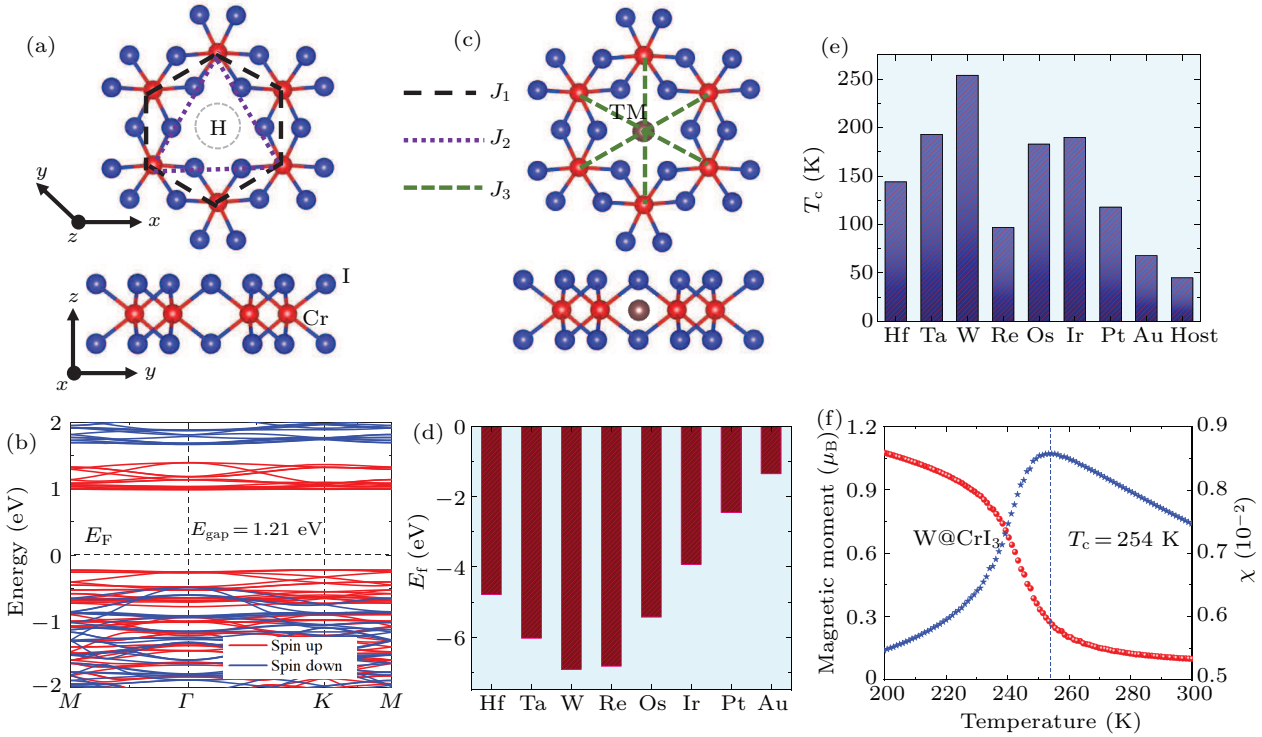


Fig. 1. (a) Top (top panel) and side (bottom panel) views of the crystal structure of CrI_3, where H represents the hollow position. (b) Calculated band structure of CrI_3. The Fermi energy is set to 0 eV. (c) Crystal structure of a transition metal (TM) atom introduced into the hollow position. (d) Formation energies of TM@CrI_3. (e) Calculated Curie temperature (T_c) of TM@CrI_3 and host CrI_3. (f) Magnetic moment and specific heat of W@CrI_3 versus temperature from Monte–Carlo simulation.

To reveal the thermodynamic stability of atomic doping, we calculate the formation energy, which is defined as $F_f = E_{dop} - E_{CrI_3} - \mu_{TM}$ where E_{dop} is the total energy of TM@CrI_3, E_{CrI_3} is the total energy of CrI_3 and μ_{TM} is the chemical potential of the TM atom. As shown in Fig. 1(d), the formation energies of all TM@CrI_3 are negative, indicat-

ing that all are thermodynamically stable. We also calculate the phonon dispersion over a $2 \times 2 \times 1$ supercell using the PHONOPY package,[37] which is based on density functional perturbation theory.[38] The absence of imaginary modes in the entire BZ is displayed in Figs. S1(a)–S1(e), indicating that monolayer TM@CrI_3 (TM = Hf, Ta, W, Re and Os) are dynamically stable. However, doping with Ir, Pt and Au atoms is not dynamically stable as the imaginary frequencies appear near the Γ point (Figs. S1(f)–S1(h)).

To estimate T_c of TM@CrI_3, we calculate exchange couplings between magnetic atoms via the Heisenberg exchange interaction, $H = \sum_{i,\delta} J_N \boldsymbol{S}_i \cdot \boldsymbol{S}_\delta$, where J_N represents the exchange couplings between magnetic atoms, i is the magnetic atomic site and δ represents the nearest neighbor distance. $\boldsymbol{S}_i$ is the spin quantum number. Here, we mainly consider the nearest and next-nearest exchange couplings between Cr^{3+} and Cr^{3+} ions as well as the nearest exchange coupling between Cr^{3+} ions and the TM atom, denoted as J_1, J_2 and J_3, respectively. J_3 is only considered for W and the Ta atoms with the larger magnetic moments. One FM and three AFM configurations (Néel, zigzag and stripy) are used in the calculations of exchange coupling, as shown in Fig. 3(a). The three magnetic coupling constants can be extracted from the following equations:

$$\begin{aligned} E_{\text{Néel}} - E_{\text{FM}} &= 24J_1\boldsymbol{S}_A \cdot \boldsymbol{S}_B + 3J_3\boldsymbol{S}_A \cdot \boldsymbol{S}_C + 3J_3\boldsymbol{S}_B \cdot \boldsymbol{S}_C, \\ E_{\text{zigzag}} - E_{\text{FM}} &= 8J_1\boldsymbol{S}_A \cdot \boldsymbol{S}_B + 32J_2\boldsymbol{S}_A \cdot \boldsymbol{S}_B \\ &\quad + 3J_3\boldsymbol{S}_A \cdot \boldsymbol{S}_C + 3J_3\boldsymbol{S}_B \cdot \boldsymbol{S}_C, \\ E_{\text{stripy}} - E_{\text{FM}} &= 16J_1\boldsymbol{S}_A \cdot \boldsymbol{S}_B + 32J_2\boldsymbol{S}_A \cdot \boldsymbol{S}_B \\ &\quad + 2J_3\boldsymbol{S}_A \cdot \boldsymbol{S}_C + 2J_3\boldsymbol{S}_B \cdot \boldsymbol{S}_C, \end{aligned}$$

where $\boldsymbol{S}_A$, $\boldsymbol{S}_B$ and $\boldsymbol{S}_C$ are the spin operators of magnetic ions on A, B and C sites. The exchange coupling constants are given in Table S1.

Based on the 2D Ising model, we employ Metropolis Monte–Carlo (MC) simulation to study T_c. Figure 1(e) shows the T_c of TM@CrI_3. T_c of the host CrI_3 is also calculated to be 45 K, which is in line with the result reported in previous work.[7] In TM@CrI_3, T_c is significantly increased. T_c of Au@CrI_3 is about 64 K, which is slightly higher than that of the host CrI_3. T_c of W@CrI_3 reaches 254 K, nearly six times higher than that of the host CrI_3, and is much increased in comparison with 3d TM@CrI_3.[29] Meanwhile, in Fig. 1(f) variation of the average magnetic moment and specific heat of W@CrI_3 with temperature is shown. We further explored T_c for W@CrI_3 for different doping concentrations: 5.9% and 8.6% represent $2 \times 2 \times 1$ CrI_3 doped with two and three W atoms, respectively (Fig. S4). It is pleasing to note that T_c of CrI_3 is significantly improved with increasing W doping concentration. As shown in Fig. 2(a), at a doping concentration of 5.9%, T_c increases from 254 K to 306 K, which is above room temperature. With continuing increase in the doping concentration, T_c of W@CrI_3 is increased to 348 K (Fig. 2(b)).

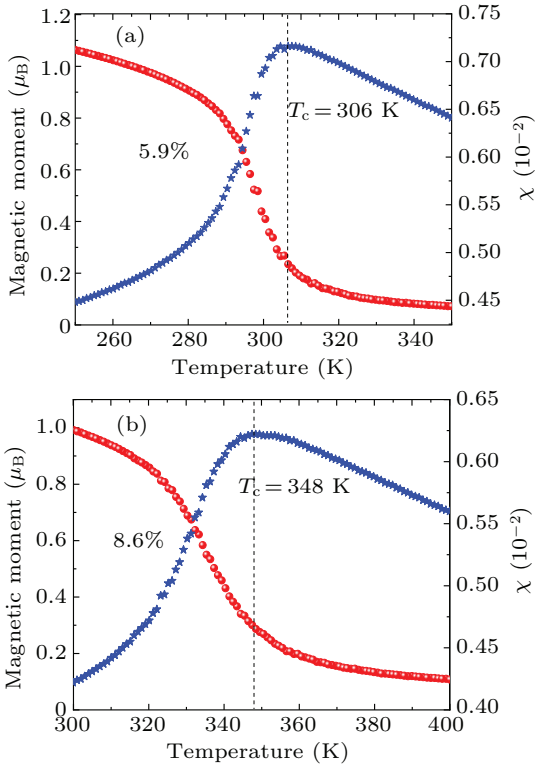


Fig. 2. Magnetic moment and specific heat versus temperature for doping concentrations of (a) 5.9% and (b) 8.6% for W@CrI_3.

To account for variation of T_c, we calculated the exchange energy, which is defined as E_{AFM}–E_{FM}. Here, zigzag-AFM is chosen as a reference due to its lower energy. Among the TM@CrI_3, the W atom has the highest exchange energy, the Ta atom the next and the Au atom the least, but their exchange energy is greater than that of CrI_3, as shown in Fig. 3(b). The pattern of variation of exchange energy is consistent with T_c. Similarly, the magnetic moments of TM atoms also show the same pattern of variation. For example, the W atom with the largest magnetic moment has the highest T_c (Fig. 3(c)). The Au atom has almost no magnetic moment, and the increase in T_c is not significant. This result indicates that T_c is related to the magnetic moments of TM atoms. The magnetic moments of TM atoms increase the exchange coupling and coordination number between the magnetic atoms. Further, according to a mean-field treatment, results for the magnetic transition temperature follow $T_c = \frac{\boldsymbol{S}(\boldsymbol{S}+1)}{3K_B}(Z_{NN}J_{NN} + \cdots)$, where Z_{NN} and J_{NN} are the coordination number and exchange coupling of magnetic atoms, respectively.[9,39] The larger the magnetic atomic coordination number, the exchange coupling and the magnetic moment, the higher the evaluated T_c. Therefore, the magnetic moments induced by doping with TM atoms can increase T_c.

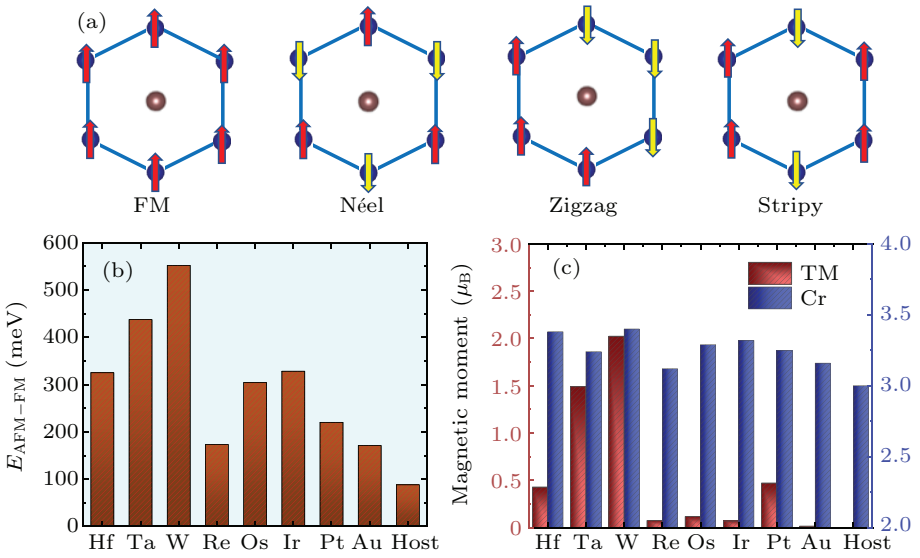


Fig. 3. (a) Four magnetic configurations: ferromagnetic (FM), Néel antiferromagnetic (AFM), zigzag AFM and stripy AFM. (b) The calculated exchange energy of TM@CrI_3 and the host CrI_3. (c) The magnetic moments of TM atoms and Cr^{3+} ions (TM, transition metal).

Next, we discuss the underlying physics of the W atomic magnetic moment in W@CrI_3. The spin-density distribution shows that the total magnetic moment stems from the Cr atoms and the W atom (Fig. 4(a)). The W atom tends to lose the partial electrons of the outermost electron shell ($5d^46s^2$) through strong electronegative action around I^- ions, and picks up a magnetic moment of about 2 μ_B. We calculated the Bader charge of W@CrI_3, where the W atom loses 0.6e and every I^- ion gains 0.11e (Table S2). In the projected density of states, d-resolved orbitals of the W atom have a large spin polarization and hybridization (Fig. 4(b)). Both the d_{xz} and d_{yz} orbitals are occupied by a fractional electron, and contribute 0.15 μ_B and 0.14 μ_B, respectively. In contrast, the d_{z^2} orbital with more spin-up electrons has a magnetic moment of 1.04 μ_B. This is because the d_{z^2} orbital rarely overlaps with the p orbitals of the surrounding I^- ions. The $d_{x^2-y^2}$ and d_{xy} orbitals protected by C_3 symmetry are degenerate below the Fermi level, and their magnetic moments are 0.35 μ_B. Furthermore, the magnitude of magnetic moments can be understood from the asymmetry of spin polarization below the Fermi level in the density of states (DOS) of TM atoms, as shown in Figs. 4(c)–4(f). For example, the spin polarized asymmetry of the Hf atom is weaker than that of the Ta atom, so the magnetic moment of the Ta atom is larger. Similarly, the W atom has a larger spin polarized asymmetry than the Ta atom, leading to a larger value for the W atom. The Os atom has the weakest asymmetry. The W atom therefore has the largest magnetic moment.

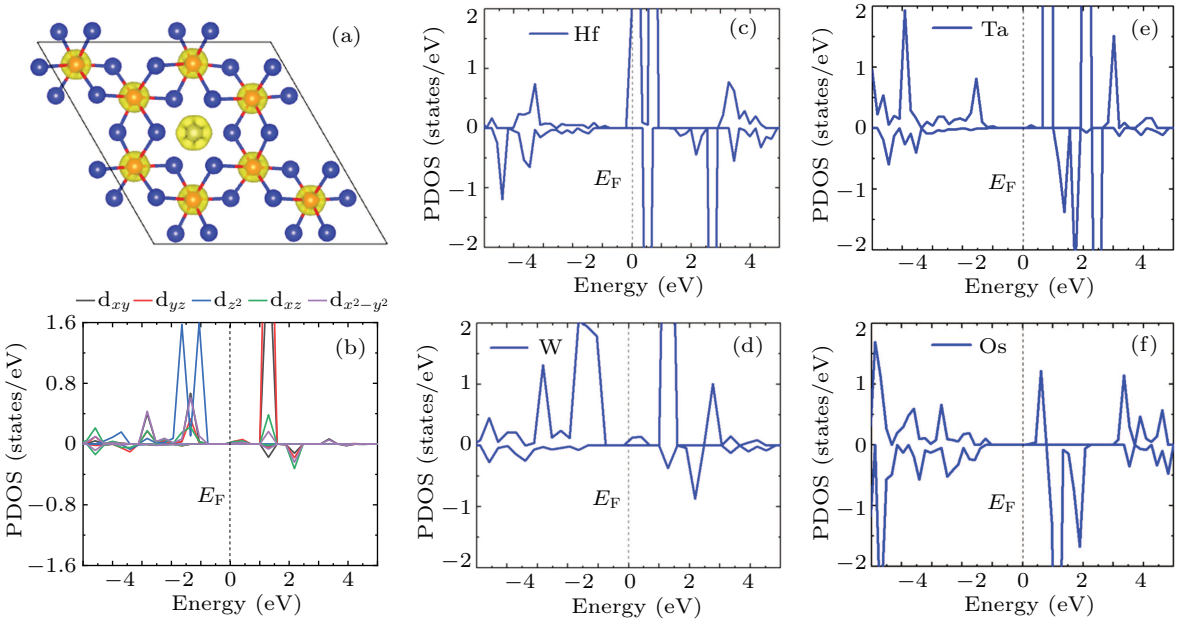


Fig. 4. (a) The spin density distribution of W@CrI_3 and (b) projected density of states (PDOS) of the W atom. Density of states (DOS) of (c) Hf, (d) W, (e) Ta and (f) Os atoms in TM@CrI_3. The positive and negative values of DOS represent spin-up and spin-down channels, respectively. The Fermi energy is set to 0 eV.

For low-dimensional materials, a large MAE driven by SOC would resist the thermal fluctuation to stabilize the long-range FM order. Due to the large SOC of 5d TM atoms, the induced MAE would be large, and is defined as $E_{\mathrm{MAE}} = E_{(100)} - E_{(001)}$. Positive or negative values of MAE represent that the magnetic easy axis is along the out-of-plane or in-plane direction, respectively. In Table 1, the magnetic easy axis of TM@CrI_3 (TM = Hf, Ta, W, Re and Ir) is along the out-of-plane direction: Re@CrI_3 has the largest MAE, which mainly originates from the Re atom. The magnetic easy axis for doping with Os, Pt and Au atoms is along the in-plane direction. Except for Os, the absolute values of MAE after doping are enhanced with respect to CrI_3, whose MAE is about 0.804 meV.[20] Therefore, doping with TM atoms can enhance the MAE of CrI_3.

Table 1. The MAE (E_{MAE}) in TM@CrI_3. The contribution from Cr, I and TM atoms is also listed. The unit is meV.

TM	E_{MAE}	Cr	I	TM
Hf	2.148	0.177	1.471	0.508
Ta	2.103	0.220	0.880	1.664
W	4.999	0.638	2.161	2.303
Re	5.910	0.352	0.797	4.861
Os	–0.437	0.398	–1.012	0.321
Ir	3.176	0.139	2.900	0.458
Pt	–5.427	0.068	–6.010	0.647
Au	–6.543	0.065	–6.811	0.225

We now discuss the FM stability of TM@CrI_3. The FM coupling of monolayer CrI_3 can be understood by the Goodenough–Kanamori–Anderson model as a competition between two exchange interactions: a direct exchange interaction between Cr^{3+} ions by electron hopping and a superexchange between the Cr^{3+} ions mediated by intermediate nonmagnetic I^- ions. As schematically shown in Fig. 5(a), stable AFM coupling depends sensitively on the distance d between Cr^{3+} ions. Stable FM coupling is dominated by superexchange interactions and is controlled by the θ of Cr^{3+}–I^-–Cr^{3+} ions. Except for the Ta atom, d of Cr^{3+}–Cr^{3+} after doping is increased with respect to the host CrI_3 (Fig. 5(b)), indicating that AFM coupling of direct exchange is weakened. The θ for all TM@CrI_3 is decreased, and is close to 90°, giving rise to stronger FM stability.

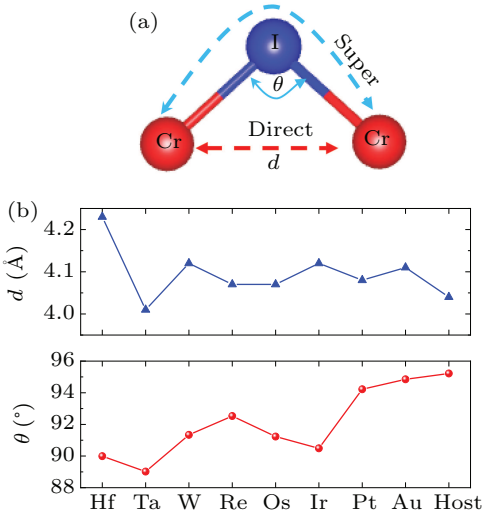


Fig. 5. (a) Diagram of direct exchange and superexchange in CrI_3. (b) The bond length d of Cr^{3+}–Cr^{3+} (top panel) and the bond angle θ of Cr^{3+}–I^-–Cr^{3+} (bottom panel).

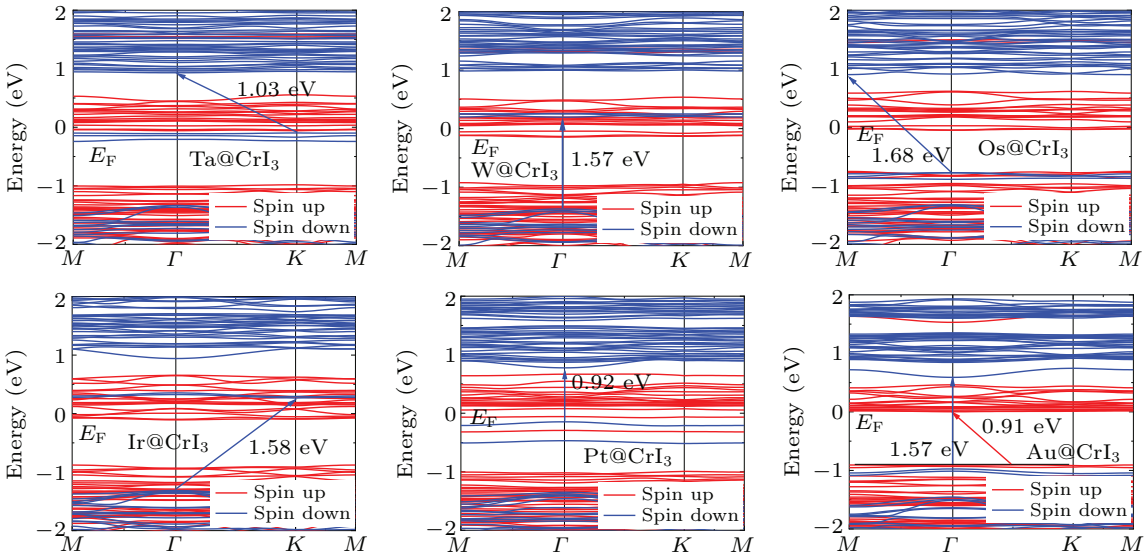


Fig. 6. The band structure of TM@CrI_3 (TM = Ta, W, Os, Ir, Pt, Au). The Fermi energy level E_{F} is set to 0 eV.

Electronic structure is a key concern in the study of physical properties. We display the band structure of TM@CrI_3 (TM = Ta, W, Os, Ir, Pt, Au) in Fig. 6. Because of the gain or loss of valence electrons (Table S3), the impurity energy levels are induced in the band structure. Therefore, the energy bands of TM@CrI_3 (TM = Ta, W, Os, Ir, Pt) cross the Fermi energy level to change from semiconductors to half-metals. Hf@CrI_3 and Re@CrI_3 are also half-metals (Fig. S6). Such

materials have promising applications in advanced magnetic recording, magnetic storage, high-efficiency magnetic sensors, spin-emitting diodes and many other fields.[40] In particular, for TM@CrI_3 (TM = W, Os, Ir), the band gaps of the spin-down channel are greater than 1.5 eV, which prevents thermal activation effects from exciting the forbidden carriers to reduce the polarization rate.[41] Au@CrI_3 is a semiconductor because the Au atom has almost no gain or loss of electrons.

4. Conclusions

In summary, we have performed a systematic study of TM@CrI_3 through the combination of a first-principles method and MC simulation. All TM@CrI_3 are thermodynamically stable due to their negative formation energy, and the absence of imaginary modes in the phonon spectra indicates that TM@CrI_3 monolayers (TM = Hf, Ta, W, Re and Os) are also dynamically stable. T_c of TM@CrI_3 is increased, with a highest value of 254 K for W@CrI_3. As the doping concentration of W atoms is increased to 8.6%, T_c is increased to above room temperature (348 K). Interestingly, W@CrI_3 has a large MAE of 4.999 meV to stabilize long-range FM order. Furthermore, the FM stability of TM@CrI_3 is enhanced. Except for doping with Au atoms, TM@CrI_3 become half-metallic. It is hoped that these results will provide theoretical guidance for experimentally tuning MAE, T_c and electronic structure.

References

[1] Novoselov K S, Geim A K, Morozov S V, Jiang D E, Zhang Y S, Dubonos S V, Grigorieva I V and Firsov A A 2004 *Science* **306** 666
[2] Mermin N D and Wagner H 1966 *Phys. Rev. Lett.* **17** 1133
[3] Lee H, Son Y W, Park N, Han S W and Yu J J 2005 *Phys. Rev. B* **72** 174431
[4] Schmidt M J and Loss D 2010 *Phys. Rev. B* **82** 085422
[5] Son Y W, Cohen M L and Louie S G 2006 *Nature* **444** 347
[6] Kan E J, Li Z Y, Yang J L and Hou J G 2008 *J. Am. Chem. Soc.* **130** 4224
[7] Huang B, Clark G, Efrén N M, Klein D R, Cheng R, Seyler K L, Zhong D, Schmidgall E, Mcguire M A and Cobden D H 2017 *Nature* **546** 270
[8] Gong C, Li L, Li Z L, Ji H W, Stern A, Xia Y, Cao T, Bao W, Wang C Z and Wang Y 2017 *Nature* **546** 265
[9] Deng Y J, Yu Y J, Song Y C, Zhang J Z, Wang N Z, Sun Z Y, Yi Y F, Wu Y Z, Wu S W and Zhu J Y 2018 *Nature* **563** 94
[10] Dillon J F and Olson C E 1965 *J. Appl. Phys.* **36** 1259
[11] Seyler K L, Zhong D, Huang B V, Linpeng X Y, Wilson N P, Taniguchi T K, Watanabe K J, Yao W, Xiao D and Mcguire M A 2018 *Nano Lett.* **18** 3823
[12] Ge M, Su Y, Wang H, Yang G H and Zhang J F 2019 *RSC Adv.* **9** 14766
[13] Jiang P H, Li L, Liao Z L, Zhao Y X and Zhong Z C 2018 *Nano Lett.* **18** 3844
[14] Sun Z Y, Yi Y, Song T, Clark G, Huang B V, Shan Y W, Wu S, Huang D, Gao C L, Chen Z H, Mcguire M, Cao T, Xiao D, Liu W T, Yao W, Xu X D and Wu S W 2019 *Nature* **572** 497
[15] Behera A K, Chowdhury S and Das S R 2019 *Appl. Phys. Lett.* **114** 232402
[16] Lee I, Utermohlen F G, Weber D, Hwang K, Zhang C, Van Tol J, Goldberger J E, Trivedi N and Hammel P C 2020 *Phys. Rev. Lett.* **124** 017201
[17] Sivadas N, Okamoto S, Xu X D, Fennie C J and Xiao D 2018 *Nano Lett.* **18** 7658
[18] Huang B, Clark G, Efrén N O, Klein D R, Cheng R, Seyler K L, Zhong D, Schmidgall E, Mcguire M A and Cobden D H 2017 *Nature* **546** 270
[19] Zhu S Z and Li T 2016 *Phys. Rev. B* **93** 115401
[20] Webster L and Yan J A 2018 *Phys. Rev. B* **98** 144411
[21] Wang R, Su Y, Yang G H, Zhang J F and Zhang S B 2020 *Chem. Mater.* **32** 1545
[22] Zhang J H, Guo Y, Li P G, Wang J, Zhou S, Zhao J J, Guo D and Zhong D H 2021 *J. Phys. Chem. Lett.* **12** 2199
[23] Pizzochero M 2020 *J. Phys. D Appl. Phys.* **53** 244003
[24] Jiang S W, Li L Z, Wang Z F, Mak K F and Shan J 2018 *Nat. Nanotechnol.* **13** 549
[25] Meng Q Y, Lu Q, Cui W B, Xu T T and Zhang L L 2022 *J. Phys. D Appl. Phys.* **55** 265303
[26] Wang H B, Fan F R, Zhu S S and Wu H 2016 *Europhys. Lett.* **114** 47001
[27] Gao Y, Wang J, Li Z P, Yang J J, Xia M R, Hao X F, Xu Y H and Gao F M 2019 *Phys. Status Solidi. Rapid Res. Lett.* **13** 1800410
[28] Guo Y, Yuan S J, Wang B, Shi L and Wang J L 2018 *J. Mater. Chem. C* **6** 5716
[29] Yang Q, Hu X H, Shen X D, Krasheninnikov A V, Chen Z and Sun L 2021 *ACS Appl. Mater. Inter.* **13** 21593
[30] Chen X, Shao Y T, Chen R, Susarla S, Hogan T, He Y, Zhang H, Wang S, Yao J, Ercius P, Muller D A, Ramesh R and Birgeneau R J 2022 *Phys. Rev. Lett.* **128** 217203
[31] Kresse G and Furthmüller J 1996 *Comp. Mater. Sci.* **6** 15
[32] Kresse G and Furthmüller J 1996 *Phys. Rev. B* **54** 11169
[33] Monkhorst H J and Pack J D 1976 *Phys. Rev. B* **13** 5188
[34] Perdew J P, Burke K and Ernzerhof M 1996 *Phys. Rev. Lett.* **77** 3865
[35] Liu L, Ren X, Xie J, Cheng B, Liu W K, An T Y, Qin H W and Hu J F 2019 *Appl. Surf. Sci* **480** 300
[36] Li T X, Jiang S W, Sivadas N K, Wang Z F, Xu Y, Weber D, Goldberger J E, Watanabe K, Taniguchi T, Fennie C J, Mak K F and Shan J 2019 *Nat. Mater.* **18** 1303
[37] Togo A and Tanaka I 2015 *Scripta Mater.* **108** 1
[38] Stefano B R, Stefano D G, Andrea D C and Paolo G N 2001 *Rev. Mod. Phys.* **73** 515
[39] Gibertini M, Koperski M, Morpurgo A F and Novoselov K S 2019 *Nat. Nanotechnol.* **14** 408
[40] Li X X and Yang J L 2017 *WIREs Comput. Mol. Sci.* **7** e1314
[41] Liu Z H, Zhang S K, Wang X, Ye X B, Qin S J, Shen X O, Lu D B, Dai J H, Cao Y Y, Chen K, Radu F, Wu W B, Chen C T, Francoual S, Mardegan J R L, Leupold O, Tjeng L H, Hu Z W, Yang Y F and Long Y W 2022 *Adv. Mater.* **34** 2200626